Lifetime measurement of excited states in the shape-phase-transitional nucleus ^{98}Zr

L. Bettermann,[1] J.-M. Régis,[1] T. Materna,[2] J. Jolie,[1] U. Köster,[2] K. Moschner,[1] and D. Radeck[1]
[1]*Institut für Kernphysik, Universität zu Köln, Zülpicherstrasse 77, D-50937 Köln, Germany*
[2]*Institut Laue-Langevin, B. P. 156, F-38042 Grenoble Cedex 9, France*
(Received 23 June 2010; published 13 October 2010)

Lifetimes of excited states in ^{98}Zr have been investigated with a $\beta\gamma\gamma$ fast-timing experiment performed at the Lohengrin mass separator at the Institut Laue-Langevin. Five lifetimes of both yrast and off-yrast states have been measured, including the lowest upper limit for $\tau(2_1^+)$. The results are compared with recent shell-model and interacting-boson-model calculations.

DOI: 10.1103/PhysRevC.82.044310 PACS number(s): 21.10.Tg, 21.10.Re, 23.20.−g, 27.60.+j

I. INTRODUCTION

In the last decade, shape-phase transitions in nuclei have been an important center of attention in nuclear-structure physics due to the proposal of two analytical solutions of the Bohr Hamiltonian, X(5) and E(5), that describe the structure of nuclei at the critical point between vibrational and deformed shapes [1,2]. The shape-phase transition in the Zr isotopic chain was described much earlier; three decades ago [3]. It occurs between the vibrational nuclei $^{92-98}$Zr and rotational nuclei $^{A\geqslant 100}$Zr where the $\nu g_{7/2}$ orbital starts to get filled. Striking evidence for coexisting shapes in the Zr and Sr isotopic chains has been described in Ref. [4]. Unfortunately, this long-recognized phase transition does not fit one of the recently found models [i.e., X(5) or E(5)]. This is due to some remarkable features in the nuclear structure of ^{98}Zr, which can be found in ^{96}Zr as well. In both nuclei, the lowest excited state is a 0^+ state. The whole region is known for its low-lying 0^+ states, which are interpreted as deformed intruder states that drop from ^{96}Zr to ^{98}Zr dramatically in energy and eventually become the ground state for $N \geqslant 60$ [5,6]. Furthermore, both nuclei show clear evidence for a subshell closure. In the case of ^{96}Zr, the $\nu d_{5/2}$ orbital is filled, which causes a sudden increase of the energy gap between the ground state and the 2_1^+ state (1751 keV). The filled $\nu s_{1/2}$ orbital in ^{98}Zr tends to result in a relatively smaller gap between the ground state and the first-excited 2^+ state at 1223 keV. However, it is still considerably larger than the 2_1^+ excitation energy in ^{92}Zr and ^{94}Zr.

Although distinct evidence for a shape transition from spherical to deformed shape was demonstrated, the complicated structural properties hinder a proper description of the Zr isotopes in the vicinity of the critical point between ^{98}Zr and ^{100}Zr in terms of the X(5) solution. Indeed, only an approach in which both normal and intruder states are taken into account, like the one of Ref. [7], would be sufficient to treat the full problem. However, calculations both within the interacting boson model (IBM), with remarkably good agreement for 0^+ and 2^+ states [8], and large-valence space shell-model (SM) calculations [9] have been performed recently. Comparison of the theoretical predictions of both models with the newly achieved data can be found in Sec. IV. The experiment and the results of the lifetime measurement are presented in Secs. II and III, respectively.

II. EXPERIMENT

The $\beta\gamma\gamma$-timing experiment was performed at the focal plane of the Lohengrin mass separator at the high-flux reactor of the Institut Laue-Langevin in Grenoble, France. Thermal-neutron-induced fission products of mass $A = 98$ generated out of a 400 μg/cm^2 ^{235}U target were selected by the mass separator. The ions were implanted into a metallized tape that was mounted in the focal plane and surrounded by the detector array. The tape was moved once per minute to remove longer-lived activity (i.e., ^{97}Zr) in mass 97 populated by β decay of ^{97}Rb and isotopes of other masses appearing at the given separator setting. The detector array consisted of a thin plastic scintillator, a LaBr$_3$(Ce) scintillation detector (LaBr) and a high-purity germanium clover detector (HPGe). The general experimental setup of $\beta\gamma\gamma$-timing experiments can be found in detail in a publication by Mach *et al.* [10]. In the framework of this article only, the essential procedure needed for the analysis is recapitulated.

In neutron-rich nuclei, β decays with relatively large transition energies can be found. Typical Q values vary between 3 and 11 MeV. In the case of β decays of low-spin isomers or ground states in the mother nuclei, low-spin states that decay through only a few γ transitions to the ground state are populated. The thin plastic scintillator mounted in the detector array measured the β-decay electrons and served as the master trigger of the setup. Additionally, the β detector set the start condition for the timing. Due to the shape of the β spectrum, the threshold for the electronic noise of the detector is not fully estimable. Therefore, the low-energy part of the β spectrum is not considered for the coincidence analysis. The deexcitation γ transitions of the β-populated state are used as the stop condition for the timing. The new and fast LaBr detectors of the array are employed, since they are ideal for this purpose [11,12]. The advantage of the new LaBr detectors, compared with the previously used BaF$_2$ scintillation detectors, is a significantly better energy resolution with similar time resolution. However, even with the better energy resolution, germanium detectors are still needed to separate the transitions of interest in the LaBr spectrum. This is done by a coincidence condition set with the HPGe clover detector. For the germanium coincidence gate, the γ transition is used that originates from the state populated by the γ transition that functions as the stop condition in the

 ©2010 The American Physical Society

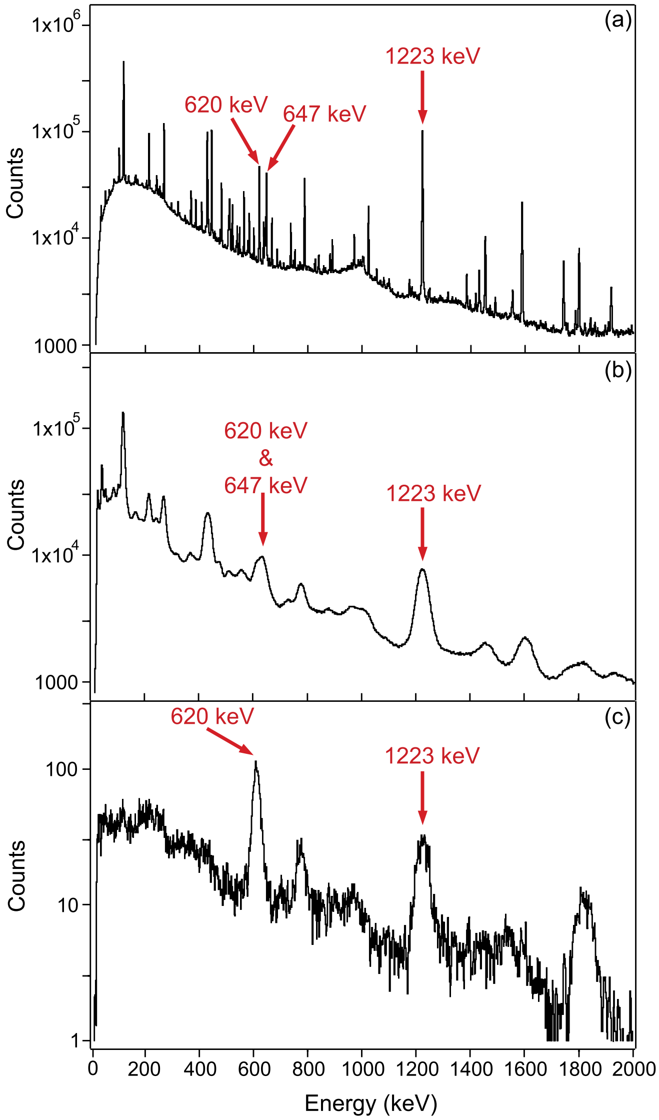

FIG. 1. (Color online) Panel (a) shows the sum of the γ-singles spectra of all four HPGe clover crystals. In panel (b), the γ-singles spectrum of the $LaBr_3$(Ce) scintillation detector (LaBr) is visible. The inferior energy resolution is evident. The $6_1^+ \rightarrow 4_1^+$ ($E_\gamma = 647$ keV), $4_1^+ \rightarrow 2_1^+$ ($E_\gamma = 620$ keV), and $2_1^+ \rightarrow 0_1^+$ ($E_\gamma = 1223$ keV) transitions are indicated by arrows. Panel (c) shows the LaBr spectrum in coincidence with the $6_1^+ \rightarrow 4_1^+$ transition ($E_\gamma = 647$ keV, gated in the HPGe spectrum). In addition, one peak originating from ^{98}Mo with an energy of 787 keV is notable. The $2_1^+ \rightarrow 0_1^+$ peak from ^{98}Mo with $E_\gamma = 787$ keV is coincident to the $2_2^+ \rightarrow 2_1^+$ transition with $E_\gamma = 645$ keV. As a cross-check, the $E_\gamma = 1432$ keV peak from the 2_2^+ state is clearly visible in the HPGe spectrum as well. The 1801-keV line originates from a state at $E = 4292$ keV in ^{98}Zr also in coincidence with the $6_1^+ \rightarrow 4_1^+$ transition. Due to the low statistic (please note the logarithmic scale of the plot) a lifetime analysis of this state was not possible.

timing. Figure 1(a) shows a sum spectrum of all crystals of the clover detector to compare the energy resolution with an energy spectrum of the LaBr detector in Fig. 1(b). Finally, in Fig. 1(c) the same spectrum as in Fig. 1(b) is presented, but this time in coincidence with the $6_1^+ \rightarrow 4_1^+$ transition gated in the clover detector.

III. RESULTS

Two different analysis methods have been used to determine the lifetime of the investigated states. Long-lived isomers with lifetimes on the order of nanoseconds and shorter are analyzed with the so-called slope technique. Due to the exponential decay behavior, a straight line can be fitted to the time spectrum plotted on a logarithmic scale. The logarithmic plot offers direct access to the lifetime of the excited states due to the linear gradient of the delayed shoulder of the peak in the time spectrum. The reciprocal of the slope is the lifetime of the state after time calibration of the spectrum. First, the lifetimes of the non-yrast states observed in the experiment, 0_3^+ and 0_4^+, are discussed. Both are known to be long-lived isomers with lifetimes on the order of several hundred picoseconds [10,13].

(i) 0_3^+ ($E = 1436$ keV): Two different values for the lifetime can be found in the literature. The first value measured with $\beta\gamma$ timing suggests a half-life of $t_{1/2} = 690 \pm 100$ ps [13], while the second value determined with $\beta\gamma\gamma$ timing results in a substantially longer half-life of $t_{1/2} = 866 \pm 40$ ps [10]. The new result achieved in this experiment of $t_{1/2} = 611 \pm 33$ ps is in a good agreement with the first value while it disagrees with the latter. Figure 2 shows the time spectrum of the $0_3^+ \rightarrow 2_1^+$ transition gated on the $2_1^+ \rightarrow 0_1^+$ transition with the clover detector. Feeding from above, in particular with an $E0$ transition from the 0_4^+ state, is negligible since the intensity of the $E0$ transition to the 0_3^+ state compared with the $E2$ transition to 2_2^+ state is only 1.3% [14]. The newly determined half-life is given as well as the other results of this experiment in Table I. For convenience, values from the literature are given, too.

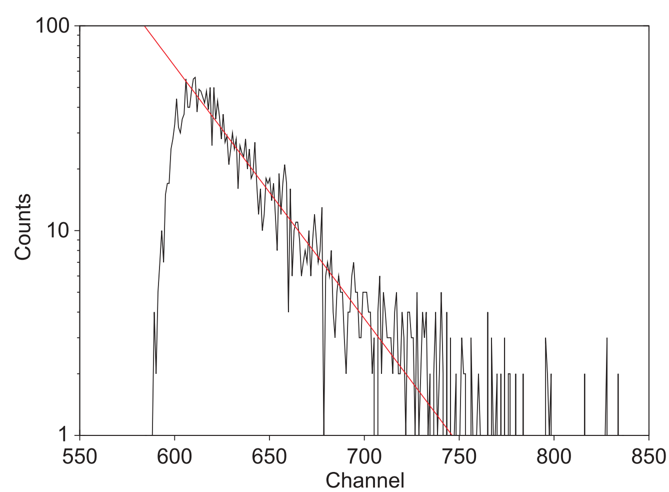

FIG. 2. (Color online) Time spectrum of the $0_3^+ \rightarrow 2_1^+$ ($E_\gamma = 1223$ keV) transition. To generate this spectrum, the clover detector was gated on the $2_1^+ \rightarrow 0_1^+$ transition. The actual fit for the determination of the lifetime was performed between channel numbers 640 and 720 and yields a half-life of $t_{1/2} = 611 \pm 33$ ps.

TABLE I. Results of the experiment in comparison with values from the literature. The level assignment follows Ref. [15].

E_{Level} (keV)	J_n^π	$t_{1/2}$ (ps)	$t_{1/2}$ (ps) [10]	$t_{1/2}$ (ps) [13]
1223	2_1^+	< 11	< 21	
1436	0_3^+	611 ± 33	860 ± 40	690 ± 100
1843	4_1^+	20 ± 6		
1859	0_4^+	318 ± 27	283 ± 15	240 ± 100
2491	6_1^+	< 10		

(ii) 0_4^+ ($E = 1859$ keV): In the literature, two values measured in the experiments introduced in the paragraph about the 0_3^+ state can be found [10,13]. Both agree within their errors ($t_{1/2} = 240 \pm 100$ ps and 283 ± 15 ps). The newly determined result of this experiment ($t_{1/2} = 318 \pm 27$ ps) is consistent with both former values within the uncertainties. The weighted mean of all three gives a value of $t_{1/2} = 292 \pm 26$ ps.

In the following paragraphs, the focus is on the yrast states. In contrast to the long-lived 0^+ isomers discussed above, the yrast states are expected to have shorter lifetimes (in the picosecond range). The slope technique for the lifetime analysis is not feasible in this case, so another technique has to be employed. Since the centroid of the peak in the time spectrum is related to the lifetime of the respective state, the so-called centroid-shift technique is used for the yrast states.

The setup itself delivers an energy dependence for the time spectrum. This means that prompt transitions at a certain energy have a certain peak position in the time spectrum; the so-called prompt position. Deexcitation transitions from states that feature a longer lifetime than the minimal resolution of the setup are shifted in the time spectrum with respect to the prompt position [16]. The difference between the prompt position at the respective energy and the peak position of the deexciting transition of the state under investigation provides the lifetime. Therefore, knowledge of the peak position of prompt transitions in the time spectrum is essential for this technique. A major difficulty in finding the prompt position is its strong energy dependence. In the past, prompt transitions with almost the same energy as the transition under investigation had to be found in order to find the prompt position of the setup at the specified energy. Recently, an empirical function was found that describes the energy dependence of the prompt position amazingly well [12]:

$$P(E_\gamma) = \frac{a}{E_\gamma + b} + c. \tag{1}$$

With the use of this function, it is now possible to find a prompt curve for the whole energy range, given that enough prompt transitions at different γ-transition energies are measured to fit Eq. (1) to the data points. In order to find the prompt curve of this setup, the nucleus ^{97}Y was measured for a few hours, since several short-lived excited states with lifetimes of $\tau \approx 5$ ps and γ transitions in different energy regions are known in ^{97}Y [17]. Figures 3(b) and 3(c) show the fit and the residuum of the fit of Eq. (1) to four prompt transitions in ^{97}Y (in black) at

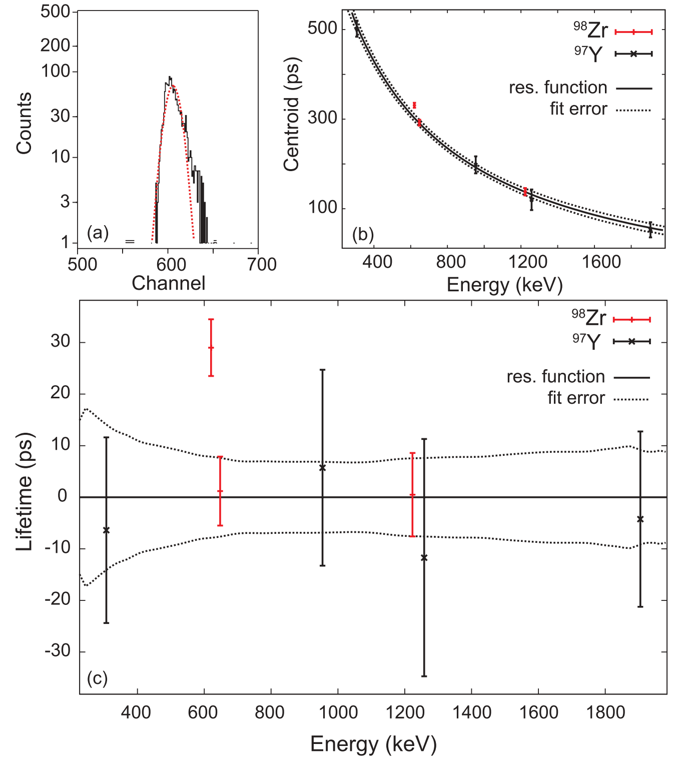

FIG. 3. (Color online) Panel (a) shows a typical time spectrum in the low picosecond range. A distinct slope on the right side of the peak is not visible. In the case presented here, the gate of the Ge clover detector was set on the $2_1^+ \rightarrow 0_1^+$ transition, while the LaBr scintillator was gated on the $4_1^+ \rightarrow 2_1^+$ transition. The timing spectrum is therefore generated by the start signal of the β-plastic detector and the stop signal of the LaBr scintillator. γ feeding from above was excluded since the lifetime of the 6_1^+ state is shorter than the timing resolution (please see paragraph on the respective state). Plot (b) shows the fit of Eq. (1) to both prompt transitions in ^{97}Y and ^{98}Zr (please see paragraphs on the 2_1^+, 4_1^+, and 6_1^+ states) and the data point of the time spectrum shown in (a). The strong energy dependence of the prompt curve is clearly visible. Panel (c) shows the residuum of the fit presented in (b). In this illustration, the lifetime of the respective states is directly visible. For instance, the $4_1^+ \rightarrow 2_1^+$ transition is at $E_\gamma = 620$ keV with a lifetime of $\tau = 29 \pm 8$ ps. In addition, the error of the fit for the respective energies is plotted.

γ-transition energies of $E_\gamma = 307,\ 954,\ 1258$, and 1904 keV. Additionally, the plots include the $2_1^+ \rightarrow 0_1^+$ and $6_1^+ \rightarrow 4_1^+$ transitions in ^{98}Zr. For details, please see the descriptions of the respective states. The centroids of the peaks in the time spectrum of the respective γ transitions were determined in the $\beta\gamma\gamma$ time spectrum. Subsequently, the channel number of the centroid position in the time spectrum was plotted against the γ-transition energy in order to fit Eq. (1) to the data.

(i) 2_1^+ ($E = 1223$ keV): The lifetime of the state is not known yet; the lowest upper limit for the lifetime of the 2_1^+ state was measured with $t_{1/2} < 21$ ps given in Ref. [10]. As described in the paragraph on the 0^+ isomers, the $\beta\gamma\gamma$ technique was used in Ref. [10] as well. In contrast to our setup, the LaBr detectors were substituted by BaF_2 detectors in their experiment. Other formerly determined upper limits are substantially longer [13,18]. The position of the peak in the $\beta\gamma\gamma$ time spectrum relative to the determined prompt curve is shown in Fig. 3(c). It has to be indicated that the fit shown in Figs. 3(b) and 3(c) has not been used for the calculation of the upper limit. Thus, the transitions $2_1^+ \rightarrow 0_1^+$ and $6_1^+ \rightarrow 4_1^+$ that are determined as prompt in what follows are already included in the fit. Instead, a fit including only the four prompt transitions of the nucleus ^{97}Y has been used for the determination of the lifetime of the 2_1^+ state. For the calculation of the upper limit ($t_{1/2} < 11$ ps), the quadratic sum of the error of the fit of Eq. (1) with the error of the peak position of the $2_1^+ \rightarrow 0_1^+$ transition was considered.

(ii) 4_1^+ ($E = 1843$ keV, $E_\gamma = 620$ keV): In a former experiment, a half-life of $t_{1/2} = 27 \pm 12$ ps was measured with the $\beta\gamma\gamma$ technique using BaF$_2$ detectors instead of LaBr [19]. Within the experimental error, this value agrees with our result of $t_{1/2} = 20 \pm 6$ ps. However, the experimental error of the result determined in our experiment is smaller. This is founded in the fact that no prompt curve was calculated in Ref. [19]. The $6_1^+ \rightarrow 4_1^+$ transition was adopted as a prompt transition, a fact proven by our experiment (see next paragraph), and then used as the prompt position for the centroid-shift analysis of the $4_1^+ \rightarrow 2_1^+$ transition. As shown in Fig. 3(b), this is not necessarily true, even at an energy in the vicinity of two γ transitions. The $\beta\gamma\gamma$-time spectrum of the $4_1^+ \rightarrow 2_1^+$ transition and the subsequent centroid-shift analysis are presented in Figs. 3(a) and 3(c), respectively. For the fit of the prompt curve, the fast transitions of the nucleus ^{97}Y have been considered as well as the $2_1^+ \rightarrow 0_1^+$ and $6_1^+ \rightarrow 4_1^+$ transitions in ^{98}Zr. Both transitions have been found to be faster than the time resolution of the setup (see the previous and next paragraphs, respectively).

(iii) 6_1^+ ($E = 2491$ keV, $E_\gamma = 648$ keV): The upper limit for the lifetime of this state was measured ($t_{1/2} < 10$ ps). The upper limit was determined to be similar to that of the 2_1^+ state. Again, only the fast transitions of the ^{97}Y nucleus were considered for the fit of the prompt curve.

IV. DISCUSSION

In the following, the newly acquired results are compared with both shell-model and IBM calculations [8,9,20]. The focus is set on the structural observables of the low-spin states, in particular the transition strengths of the 2_1^+ and 4_1^+ states. Experimental and theoretical transition strengths can be found in Table II.

A. Shell model

The codes NATHAN [21] and ANTOINE [22] were used for the calculations. For the NN interaction, the Bonn-C and the CD-Bonn potentials have been employed with an adjustment of the two-body matrix elements to Ni isotopes with $A = 57 - 78$ and $N = 50$ isotones (^{79}Cu–^{100}Sn). For the $E2$ transition rates, enhanced effective charges for protons and neutrons ($e_{\text{eff}}^{\nu} = 0.8$ eb and $e_{\text{eff}}^{\pi} = 1.8$ eb) deviating from standard values ($e_{\text{eff}}^{\nu} = 0.5$ eb and $e_{\text{eff}}^{\pi} = 1.5$ eb) were used. The necessity of increased effective charges is a general issue in this region, even with other potentials (see, e.g., Ref. [23] with $e_{\text{eff}}^{\nu} = 1.5$ eb and $e_{\text{eff}}^{\pi} = 1.8$ eb). For further details of the calculation presented here and, in particular, for the truncation in the model space, please see the original article [9].

TABLE II. Experimentally determined transition rates compared to the shell-model calculation from Refs. [9,20] and the IBM calculations performed with parameters given in Ref. [8], except for the effective charge e_{eff}. In contrast to the calculation in [8], in which e_{eff} was fixed to reproduce the $B(E2; 2_1^+ \rightarrow 0_1^+)$ value in ^{100}Zr, the $2_1^+ \rightarrow 0_1^+$ transition strengths in ^{94}Zr was chosen. This results in a value of $e_{\text{eff}} = 0.077$ eb for the effective charge.

Transition	Exp. (e^2fm^4)	SM (e^2fm^4)	IBM (e^2fm^4)
$B(E2;\, 2_1^+ \rightarrow 0_1^+)$	> 19	70.4	349
$B(E2;\, 4_1^+ \rightarrow 2_1^+)$	294 ± 81	68.95	483

The excitation energies of the low-spin states, except for the 3^- state, are very well reproduced by the calculation (see Fig. 11 in [9]), in contrast to the transition strengths as far as comparable. The $B(E2;\, 4_1^+ \rightarrow 2_1^+)$ value of 69 e^2fm^4 highly underestimates the experimental value of 294 ± 81 e^2fm^4. The proposed $B(E2;\, 2_1^+ \rightarrow 0_1^+) = 70.4$ e^2fm^4 value would result in a lifetime of approximately $\tau = 4$ ps for the 2_1^+ state.

B. Interacting boson model

In the simplest version of the IBM, valence nucleons are treated pairwise as bosons with angular momentum 0 (s) and 2 (d), respectively. Even-even nuclei are particularly well suited for the description in the IBM. The four-parameter Hamiltonian of the extended consistent Q formalism (ECQF) [24–26] enhanced with an angular momentum term was used in this study:

$$\hat{H} = \epsilon \hat{n}_d - \kappa(\hat{Q}^\chi \cdot \hat{Q}^\chi) + \kappa'(\hat{L} \cdot \hat{L}). \tag{2}$$

It consists of a single-boson energy term in which the d-boson number operator is indicated through $\hat{n}_d$ and the quadrupole and angular momentum operators through

$$\hat{Q}^\chi = s^\dagger \tilde{d} + d^\dagger s + \chi [d^\dagger \tilde{d}]^{(2)} \tag{3}$$

and

$$\hat{L} = \sqrt{10}\,(d^\dagger \tilde{d})^{(1)}, \tag{4}$$

respectively. The $E2$ transition operator exhibits the same structure as the quadrupole operator, $Q(E2) = e_{\text{eff}} \cdot \hat{Q}$ with e_{eff} as the effective charge.

For the boson number, only the neutrons from a ^{90}Zr core, due to shell closures at $N = 50$ and $Z = 40$, are taken into account. Therefore, the total boson number is $N_B = 4$. The additional parameter values for ^{98}Zr are $\epsilon = 0.380$, $\kappa = 0.032$, $\chi = -0.8$, and $\kappa' = 0.15$ [8].

The overall agreement of excitation energies of the low-spin states is noteworthy for the Zr isotopic chain and, in particular, for the rotational nuclei with $A \geqslant 100$ and

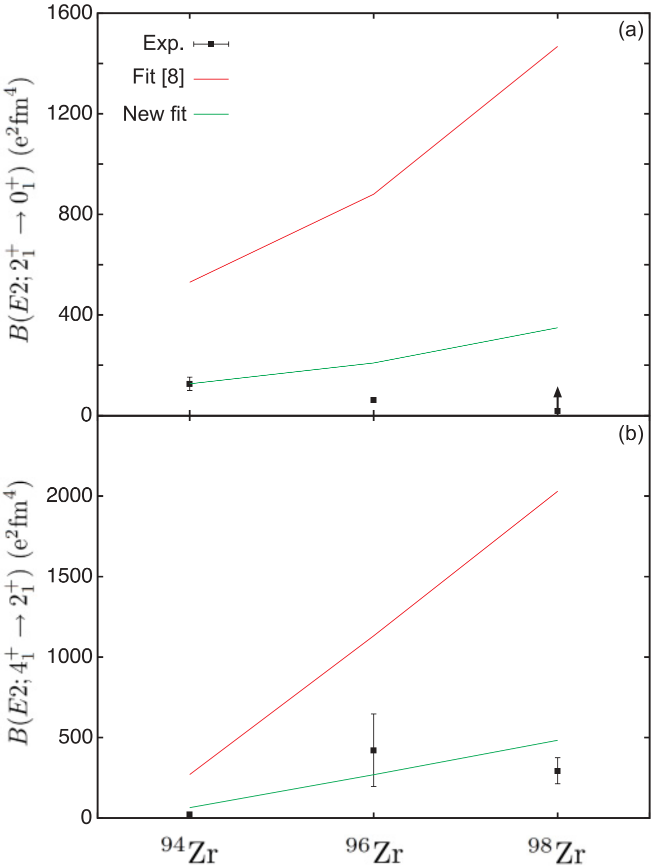

FIG. 4. (Color online) Comparison of calculated transition strength with experimental data for the vibrational Zr isotopes. The red curves show the transition strengths achieved with an effective charge of $e_{\mathrm{eff}} = 0.159$ eb, which was fit to the $B(E2;\, 2^+_1 \rightarrow 0^+_1)$ value in ^{100}Zr [8]. The transition strengths plotted in green are calculated with the smaller effective charge of $e_{\mathrm{eff}} = 0.077$ eb (see text).

the vibrational nuclei. For ^{98}Zr, the 2^+_1 and 2^+_2 states are reproduced almost exactly by the fit. The 4^+_1 state is off, but still in the vicinity of the experimental value. However, the theoretically determined excitation energy of the 6^+_1 state is far beyond reasonable energies.

For the transition strengths, the effective charge $e_{\mathrm{eff}} = 0.077$ eb has been modified from the original value used in Ref. [8] ($e_{\mathrm{eff}} = 0.159$ eb) because the effective charge was fit in that work to the transition strengths in ^{100}Zr. For rotational bands in Zr nuclei with $N \geqslant 60$, the effective charge from Ref. [8] works fine but, for the spherical nuclei between ^{92}Zr and ^{98}Zr, the theoretical $B(E2)$ values strongly overestimate the experimental values. This decrease of the effective charge for the lighter isotopes is founded in the disappearance of the $Z = 40$ subshell closure at ^{100}Zr. In deformed nuclei, the $B(E2;\, 2^+_1 \rightarrow 0^+_1)$ value is proportional to e_{eff}. A doubling of the boson number (from $N_B = 5$ with the $Z = 40$ subshell to $N_B = 10$ without the $Z = 40$ subshell, in the case of ^{100}Zr) is compensated by taking half of the effective charge. The effective charge used in this work is achieved by fitting the $B(E2;\, 2^+_1 \rightarrow 0^+_1)$ value in ^{94}Zr. This describes all low-spin transition strengths of the spherical nuclei considerably better, as shown in Fig. 4. Isotopes of Zr with $N \geqslant 60$ are not given in the plot since the parameters of Eq. (2) are fit with an existing $Z = 40$ subshell closure in [8].

For ^{98}Zr, the calculated value $B(E2;\, 4^+_1 \rightarrow 2^+_1) = 483\ e^2$fm^4 is just outside the experimental error. Similar to the shell model calculation, the predicted transition strength of the 2^+_1 state to the ground state is used to estimate the lifetime. For the IBM calculation, this results in a lifetime of approximately $\tau = 0.65$ ps for the 2^+_1 state.

V. CONCLUSION

Four lifetimes of excited states in the phase-transitional nucleus ^{98}Zr have been remeasured and, additionally, an upper limit for the lifetime of one state (6^+_1) was obtained. For the lifetime of the first 2^+ state, only an upper limit ($\tau < 16$ ps) was measured. Model predictions for the lifetime of this state are between approximately $\tau = 0.65$ ps (IBM) and $\tau = 4$ ps (SM). The transition strengths of the $4^+_1 \rightarrow 2^+_1$ transition achieved from the IBM with a reduced effective charge is in very good agreement with experiment.

Further experiments on the lifetime of excited states in ^{98}Zr, in particular of the 2^+_1 state, are absolutely necessary for the test of model predictions. The knowledge of the "missing" $B(E2;\, 2^+_1 \rightarrow 0^+_1)$ value in the Zr isotopic chain and therefore the evolution of deformation along the chain would lead to a deeper understanding of the shape-phase transition around $A \approx 100$ and would give access to further studies of the $\nu g_{7/2}$–$\pi g_{9/2}$ interaction.

ACKNOWLEDGMENTS

We are grateful to S. Heinze and A. Blazhev for fruitful discussions and to to K. Sieja for the courtesy of additional information on the shell-model calculations. This work was supported by the German BMBF under grant number O6KY205I.

[1] F. Iachello, Phys. Rev. Lett. **85**, 3580 (2000).
[2] F. Iachello, Phys. Rev. Lett. **87**, 052502 (2001).
[3] P. Federman and S. Pittel, Phys. Rev. C **20**, 820 (1979).
[4] H. Mach, M. Moszynski, R. L. Gill, F. K. Wohn, J. A. Winger, J. C. Hill, G. Molnár, and K. Sistemich, Phys. Lett. B **230**, 21 (1989).
[5] K. Heyde, P. V. Isacker, R. F. Casten, and J. L. Wood, Phys. Lett. B **155**, 303 (1985).
[6] K. Heyde, J. Jolie, J. Moreau, J. Ryckebusch, M. Waroquier, P. V. Duppen, M. Huyse, and J. L. Wood, Nucl. Phys. A **466**, 189 (1987).
[7] A. Frank, P. Van Isacker, and F. Iachello, Phys. Rev. C **73**, 061302 (2006).
[8] J. Garcia-Ramos, K. Heyde, R. Fossion, V. Hellemans, and S. D. Baerdemacker, Eur. Phys. J. A **26**, 221 (2005).

[9] K. Sieja, F. Nowacki, K. Langanke, and G. Martínez-Pinedo, Phys. Rev. C **79**, 064310 (2009).
[10] H. Mach, R. Gill, and M. Moszynski, Nucl. Instrum. Methods A **280**, 49 (1989).
[11] J.-M. Régis *et al.*, Nucl. Instrum. Methods A **606**, 466 (2009).
[12] J.-M. Régis, G. Pascovici, J. Jolie, and M. Rudigier, Nucl. Instrum. Methods A **622**, 83 (2010).
[13] K. Kawade, G. Battistuzzi, H. Lawin, H. Selic, K. Sistenich, F. Schussler, E. Monnand, J. Pinston, B. Pfeiffer, and G. Jung, Z. Phys. A **304**, 293 (1982).
[14] G. Lhersonneau *et al.*, Phys. Rev. C **49**, 1379 (1994).
[15] G. S. Simpson *et al.*, Phys. Rev. C **74**, 064308 (2006).
[16] W. Andrejtscheff, M. Senba, N. Tsoupas, and Z. Ding, Nucl. Instrum. Methods **204**, 123 (1982).
[17] M. Büscher, R. F. Casten, R. L. Gill, R. Schuhmann, J. A. Winger, H. Mach, M. Moszyński, and K. Sistemich, Phys. Rev. C **41**, 1115 (1990).
[18] I. Ahmad *et al.*, ANL Phys. Div. Rep. **2000**, 24 (2001).
[19] M. Liang, Ph.D. thesis, University of Cologne, 1992.
[20] K. Sieja (private communication).
[21] E. Caurier, G. Martinez-Pinedo, F. Nowacki, A. Poves, and A. P. Zucker, Rev. Mod. Phys. **77**, 427 (2005).
[22] E. Caurier and F. Nowacki, Acta Phys. Pol. B **30**, 705 (1999).
[23] A. Holt, T. Engeland, M. Hjorth-Jensen, and E. Osnes, Phys. Rev. C **61**, 064318 (2000).
[24] D. D. Warner and R. F. Casten, Phys. Rev. Lett. **48**, 1385 (1982).
[25] P. O. Lipas, P. Toivonen, and D. D. Warner, Phys. Lett. B **155**, 295 (1985).
[26] V. Werner, N. Pietralla, P. von Brentano, R. F. Casten, and R. V. Jolos, Phys. Rev. C **61**, 021301 (2000).